Invited Paper, State-of-the-Art Program on Compound Semiconductors (SOTAPOCS XXV)
190th Electrochemical Society Meeting, San Antonio, TX, October 6-11, 1996

GROWTH OF VERTICAL-CAVITY SURFACE EMITTING LASERS BY METALORGANIC VAPOR PHASE EPITAXY

H. Q. Hou, B. E. Hammons, M. H. Crawford, K. L. Lear, and K. D. Choquette
Sandia National Laboratories, MS 0603, Albuquerque, NM 87185, U.S.A.

We present the growth and characterization of visible and near-infrared vertical-cavity surface emitting lasers (VCSELs) grown by metalorganic vapor phase epitaxy. Discussions on the growth issue of VCSEL materials include the growth rate and composition control using an *in situ* normal-incidence reflectometer, comprehensive *p*- and *n*-type doping study in AlGaAs by CCl_4 and Si_2H_6 over the entire composition range, and optimization of ultra-high material uniformity. We will also demonstrate our recent achievements of all-AlGaAs VCSELs which include the first room-temperature continuous-wave demonstration of 700-nm red VCSELs and high-efficiency and low-threshold voltage 850-nm VCSELs.

INTRODUCTION

Vertical-cavity surface emitting lasers (VCSELs) are promising for a variety of applications such as optical interconnects and communications, laser printing, recording, and displays.[1] The growth of VCSELs, however, is very demanding. The thickness and composition control has to be accurate enough to align the mirror reflectance wavelengths of the top and bottom distributed Bragg reflectors (DBRs), the gain spectrum, and cavity resonance wavelength to a specific wavelength regime. In addition, the composition and doping level across the interfaces of the high- and low-index DBR constituents often need to be graded continuously to reduce the device series resistance. Metalorganic vapor phase epitaxy (MOVPE) technology appears to be a superior growth platform because of the ability to accomplish these with high throughput. However, the control of the composition, layer thickness, and doping level can be complicated. In this paper, we will present the critical issues and optimization for growth of high-quality VCSEL materials.

GROWTH OF VCSELs

Epitaxial growth was performed in an EMCORE GS3200 MOVPE rotating disk reactor. GaAs and $Al_xGa_{1-x}As$ were grown at 750°C by using trimethylgallium (TMG), trimethylaluminium (TMA), and 100% arsine (AsH_3). Dopants for *n*- and *p*-type materials were from disilane (Si_2H_6) and carbon-tetrachloride (CCl_4), respectively. The alkyl and doping precursors were mixed in an injection block, and carried by high-purity H_2 to the EMCORE vertical reactor through 3 different injection zones distributed along the radial direction on the top flow-injection flange. The AsH_3 was injected through two other zones. The reactants were isolated from the stainless steel chamber wall with a high hydrogen flow along the shroud. Therefore, there is little up-stream contamination or

DISCLAIMER

carryover to a substrate. The substrate was rotated at 1000 rpm. The reactor pressure was 60 torr.

1. Growth Rate and Composition Determination by In situ Reflectometer

In the past, the versatility of the MOVPE technology has been compromised due to the lack a suitable *in situ* pregrowth calibration tool. The traditional geometry of the MOVPE reactor prohibits the use of *in situ* tools, such as pyrometric interferometry and ellipsometry which are commonly used in a molecular beam epitaxy (MBE) system for growth monitoring. Slight day-to-day variation can drift the VCSEL wavelength and change the laser characteristics significantly since the control of growth rate, composition, and doping are so critical for VCSELs. The MOVPE growth conditions are usually determined in advance through an often tedious set of calibration runs. We employed an *in situ* technique by normal-incidence reflectometer for pregrowth growth-rate and composition calibration and real-time growth monitoring.

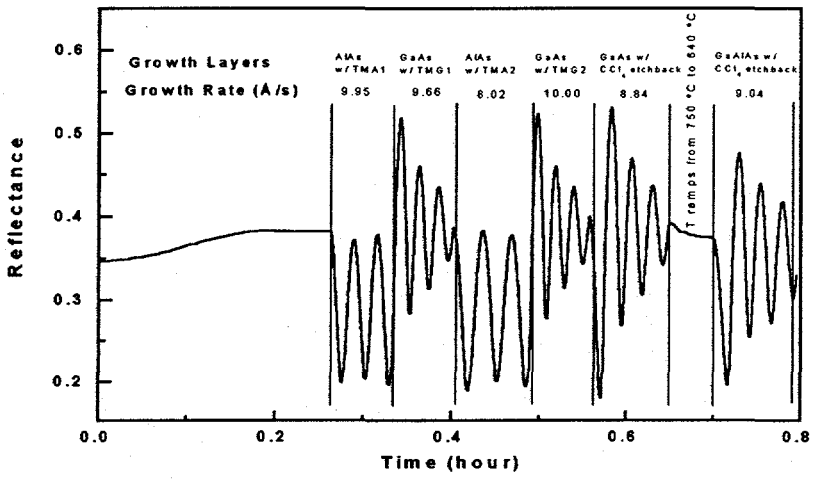

Fig. 1. Temporal reflectance of a typical calibration run for the growth rate and etchback rate during AlGaAs growth. The alloy composition can be linearly interpolated. Within an hour, growth and etchback rates are obtained for the various growth conditions.

The normal-incidence reflectance setup consists of a 7-watt W-halogen lamp as the light source and a silicon detector with a 10 nm bandwidth interference filter at 633 nm to detect the reflectance signal. The whole assembly was mounted directly on the top miniflange window of the reactor. A virtual interface model[2] extracts the growth rate and optical constants from the absolute reflectance of only the topmost layer by referencing the starting signal to the known reflectance of the substrate before epitaxy begins. It does not require any knowledge of epitaxial materials, interface position, thickness, or composition of underlying epitaxial layers. This provides a simple, robust, and accurate measurement of the growth rate.[3] Shown in Fig. 1 is the temporal reflectance from a typical calibration run. The growth rates achieved by using various alkyl sources were determined from fitting the reflectance waveform with the virtual interface model. The alloy composition can be linearly interpolated since the growth rate is mostly

mass transport limited. The reduction of the growth rate due to an etchback effect of AlGaAs by CCl_4 with different C doping levels at different temperatures is also extracted from this single calibration run of less than an hour.[3] The small deviation of the growth rate from the expected value was therefore corrected afterwards.

2. Carbon Doping and Etchback Effect in AlGaAs

One of the critical growth issues is to dope DBRs just enough to achieve low series resistance and also keep the free-carrier absorption low. Carbon is a very attractive *p*-type dopant for GaAs and AlGaAs due to its low activation energy, good electrical activity, low diffusivity, and high solid solubility.[4] However, the utility of CCl_4 as a doping source brings parasitic etching reactions by Cl radicals which reduce the growth rate. We have performed an extensive study of the C doping efficiency by CCl_4 in AlGaAs over the entire range of Al composition. Shown in Fig. 2 is the carrier concentration and etchback rate as a function of the CCl_4 partial pressure in GaAs at 640 °C. The free carrier concentration from Hall measurements is almost linearly dependent on the flow rate or partial pressure of the CCl_4. This implies that there is no self-compensation process in C doping. A large dynamic range from 10^{16} to high 10^{19} cm^{-3} doping can be achieved routinely with excellent surface mophorlogy at this temperature. A higher doping level could be obtained by using higher CCl_4 partial pressure at lower growth temperature.

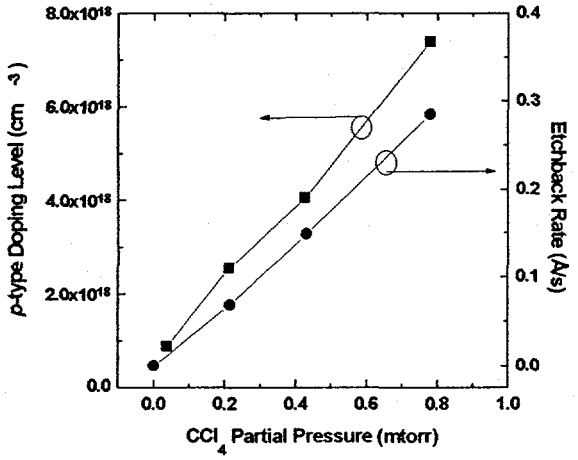

Fig. 2 Carrier concentration and etching rate in GaAs at 640 °C as a function of the CCl_4 partial pressure.

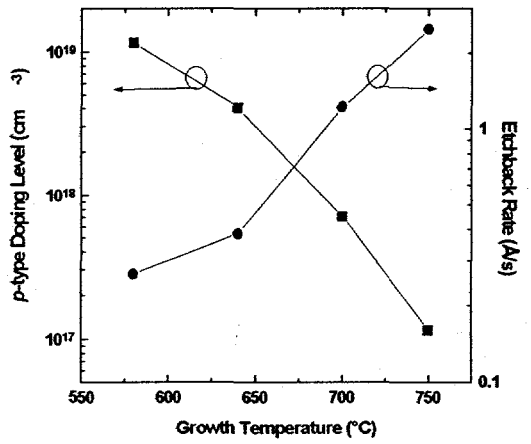

Fig. 3 Carrier concentration and etching rate in GaAs as a function of the growth temperature.

The etchback rate as measured from the *in situ* reflectance[3] is the difference of the growth rates when the film was grown with the C doping and without the C-doping. This is plotted in Fig. 2 on the right y-axis during GaAs growth at 640 °C. The etchback rate is almost proportional to the CCl_4 partial pressure.

Both the doping efficiency and etchback rate are found to be very dependent on the growth temperature. Figure 3 shows the carrier concentration and etching rate as a function of the growth temperature for GaAs with a fixed CCl_4 partial pressure of 0.43 mtorr. The doping efficiency decreases by two orders of magnitude when the growth

temperature varies from 580 to 750 °C. On the other hand, as shown by the right y-axis in Fig. 3, the etching rate increases by an order of magnitude when the growth temperature changes from 580 to 750 °C. Therefore, it is generally better for achieving a higher doping level with a lower growth temperature where the etchback rate is much lower. Another noteworthy feature shown in Fig. 3 is that the doping level can change by 30 to 40% if the growth temperature varies 20 °C. Therefore, the growth temperature is also crucial for achieving uniform and reproducible C doping in AlGaAs.

The experiment was furthered by doping C in AlGaAs with aluminum composition ranging from 0 to 1 when the same CCl_4 flow rate or partial pressure is maintained. The doping level changes from 2×10^{17} to 2×10^{19} cm^{-3} when the Al composition in AlGaAs changes from 0 to 1 even with the same CCl_4 flow and growth temperature (750 °C), as shown in the left-axis of Fig. 4. Therefore, if a constant doping level is to be maintained, the CCl_4 flow rate has to be varied accordingly. Furthermore, the right y-axis in Fig. 4 shows that this etchback rate has a strong dependence on Al composition in AlGaAs. The etchback rate for GaAs is approximately 15 times higher than that for AlAs. This selectivity versus Al composition in AlGaAs has a direct implication on bandgap, refractive index, and conductivity engineering in the lateral direction with a prepatterned substrate and performing *in situ* selective etching.[5]

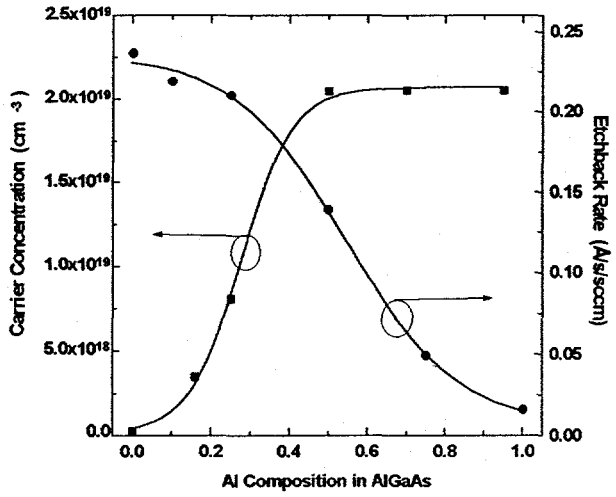

Fig. 4 Carrier concentration and etching rate for AlGaAs with different Al composition when the CCl_4 flow rate is kept the same.

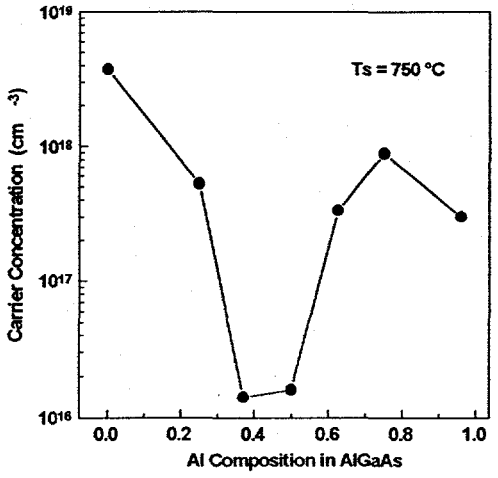

Fig. 5 Free carrier concentration in Si-doped AlGaAs grown at 750 °C as a function of the Al composition when the Si_2H_6 flow rate is kept the same.

The above-studied doping and etching behavior can be understood as follows. The C has to be incorporated on the As site to be a *p*-type dopant. However, the Cl may bond with Ga or Al atoms, and form volatile $GaCl_3$ and $AlCl_3$. This will in turn make the doping inefficient since more Ga or Al will be pulled away which will otherwise allow C to be incorporated. Thus, more etchback and less efficient doping results from the same mechanism. Since such a reaction between Cl and Ga (Al) is expected to be more

significant at higher temperature, this will lead to a faster etchback rate and more inefficient C doping as we see from the experiment. On the other hand, the Al-C bond is stronger than the Ga-C bond, and $AlCl_3$ is less volatile than $GaCl_3$. Thus, the etchback rate is slower for AlAs than for GaAs, and the C can be more readily doped into AlAs than in GaAs. This accounts for the strong dependence of the doping level and etchback rate on the Al composition in AlGaAs.

3. Silicon as an n-type Dopant in AlGaAs

The *n*-type doping in AlGaAs was achieved with Si_2H_6. It is found that the Si doping efficiency is not very temperature dependent in the growth temperature range from 640 to 750 °C. Figure 5 shows the carrier concentration from Hall measurements as a function of the Al composition in AlGaAs doped with the same flow of Si_2H_6 of 0.73 sccm. The free carrier concentration in GaAs is approximately 4 times higher than in AlAs, and a drop of two orders of magnitude occurs at an Al composition of about 0.45. On the other hand, the polaron measurements showed the same doping concentration of Si in AlGaAs in the entire composition range. Therefore, the low carrier concentration in the vicinity of $x = 0.45$ is due to insufficient activation. This drop can be well correlated to a sudden increase of the activation energy of Si in AlGaAs with $x \sim 0.45$, which is due to the transition of the conduction bandege of AlGaAs from direct to indirect around this composition range.[6] Furthermore, the conduction bandedge transition from Γ to X band gives rise to an increase of the electron effective mass, which results in a deficient activation of the *n*-type dopant. An attempt to increase the doping concentration may not lead to an increase of free carrier concentration since the Si dopant can be substitutional but not activated or interstitial. The presence of a large concentration of interstitials, however, should produce significant outdiffusion during post-growth processing and device operation. This may cause device reliability problems. Therefore, a mirror design which skips the Al composition range of insufficient *n*-dopant activation should be beneficial to a reliable low-series resistance.

MATERIAL UNIFORMITY

The sample uniformity was optimized by changing the gas-flow partition for alkyl sources among the three injection zones with the hydride flow partition of 80%:20% between the inner and outer injection zones and a total reactor flow of 32.6 slm. Mirror structures of 20-period of AlGaAs/AlAs DBRs were grown under different conditions. The center wavelength of the DBR reflectivity stopband was measured for different radial positions of a 3" diameter wafer. It is found that equal alkyl distribution among the three injection zones on the top flange did not give a uniform growth rate on the substrate. Instead, a setting of the gas-flow distribution of 7%:78%:15% between the inner, middle, and outer injection zones yielded the most uniform thickness. The uniformity, which is most sensitive to the partition setting, was further optimized with the AsH_3 flow rate, or the V/III ratio. We found that the uniformity can be tuned slightly with AsH_3 flow rates from 230 to 270 sccm, or the equivalent V/III ratio from 36 to 42.3, and the best

uniformity across an entire 3" wafer was achieved with an AsH_3 flow of 248.5 sccm, or a V/III ratio of approximately 39.

Figure 6 shows the wavelength of the Fabry-Perot cavity mode for an 850-nm VCSEL structure grown with the above-optimized conditions as a function of the distance from the wafer center. The uniformity was found to be rotation symmetric except for a little disturbance near the major flat of the wafer. The wavelength for the area ~3 mm from the wafer edge (the last data point in Fig. 6) can be slightly influenced by the thickness of material coated on the susceptor. The wavelength variation ($\Delta\lambda$) was measured to be 0.8 nm in the center 2" and 3.3 nm across the entire 3" wafer. This corresponds to a wavelength and thickness uniformity of ±0.05% in the center 2" area of the 3" wafer, and ±0.2% over the entire 3" wafer. Since the alkyl gases are mixed uniformly before being injected into the reactor, and the incorporation ratio of Al/Ga is fairly insensitive to a small temperature variation around 750 °C, the composition variation across a wafer should be negligible. This uniformity result is believed to be among the best achievable for III/V semiconductor epitaxial technology for an entire 3" wafer area.[9]

The MOVPE growth runs are also highly reproducible when a pregrowth calibration with the *in situ* reflectance is performed about once every 20~30 runs. We obtained wavelength run-to-run reproducibility of ±0.3% for both 770- and 850-nm VCSELs in the course of over 100 runs. [9].

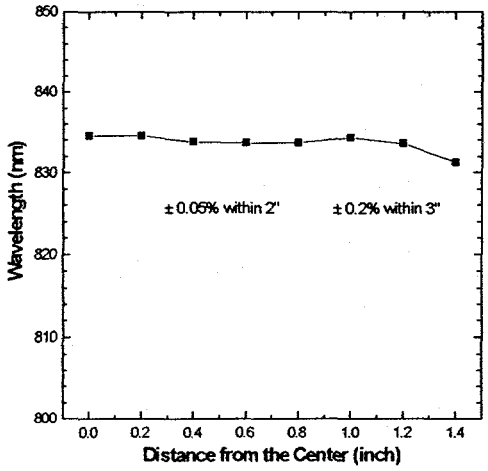

Fig. 6. Wavelength of the Fabry-Perot cavity mode for an 850-nm VCSEL as a function of the distance from the wafer center.

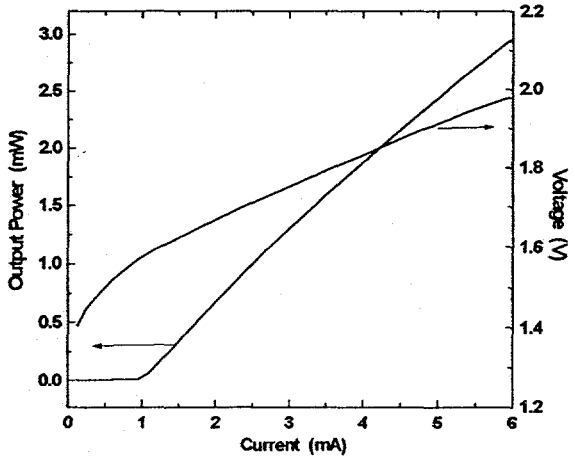

Fig. 7. L-I-V curves for an oxide-confined aperture VCSEL. The threshold voltage is 1.58 V, and wall-plug efficiency is 26%.

DEVICE PERFORMANCE

A typical VCSEL sample consists of Si-doped *n*-DBR mirrors with high reflectivity, one-wave thick optical cavity composed of cladding layers with linear composition and doping ramping and quantum well active range, and C-doped *p*-DBR mirrors. A half-wave thick highly-doped (~3×10^{19} cm^{-3}) current spreading layer caps the

whole structure. In the DBR layers, the composition was parabolically graded across the interfaces of high and low Al-containing layers to reduce the series resistance. The doping profile in the DBR mirrors was optimized based on the *p*- and *n*-type doping studies. We have performed a simple one-dimensional Possion-Schrodinger equation to calculate the band diagram. It is found that the energy spike at the heterointerface can be reduced significantly by employing a parabolic composition ramping. As a result, the series resistance is greatly reduced compared to an abrupt and piece-linear ramping profiles of the DBR interfaces.[7] A further improvement can be achieved by modulating the doping profile to compensate the band bending.

The standard procedures for device isolation include etched air post and proton-implantation. Recently, the process of selective oxidation yielded a significant improvement for device performance. AlGaAs with high Al composition can be converted to a stable oxide, and the oxidation rate of AlGaAs in a hot steam ambient is very dependent on the Al composition. For instance, the oxidation rate of $Al_{0.98}Ga_{0.02}As$ is 3.5 times higher than $Al_{0.92}Ga_{0.08}As$.[8] Therefore, if the low-index layer of a DBR mirror contains $Al_{0.92}Ga_{0.08}As$ for most of the DBR structure, and only leaves one period of $Al_{0.98}Ga_{0.02}As$ layer close to the cavity, this layer can be selectively oxidized to form a current aperture. The typical oxidation rate for $Al_{0.98}Ga_{0.02}As$ layers was approximately 0.8 μm/min at 440 °C. The size of the devices can be easily controlled by the oxidation depth from the side.

1. High Efficiency and Low-threshold Voltage 850 nm VCSELs

Figure 7 shows typical output power-current (L-I) and voltage-current (V-I) curves from a room-temperature continuous-wave (CW) 850-nm VCSEL. The device contains 5 GaAs(80 Å)/$Al_{0.2}Ga_{0.8}As$ quantum wells and 35 periods of $Al_{0.92}Ga_{0.08}As$/ $Al_{0.16}Ga_{0.84}As$ *n*-DBRs and 20 periods of *p*-DBRs, and was processed by selective oxidation. The oxide aperture size is ~ 8×8 μm^2. The threshold voltage is measured to be 1.58V. This is only ~100 meV above the photon energy. The differential resistance is ~80 Ω even for this small-aperture oxide device. The voltage drop is less than 2V even when the output power is 3 mW. The threshold current is about 1 mW, and the slope efficiency is as high as 0.6 W/A. The wallplug efficiency is calculated to be ~ 26%, which is very high. These devices are also highly uniform across the entire 3" wafer. The total variation of the lasing wavelength is 5 nm around 844 nm. This corresponds to a lasing wavelength uniformity of ±0.3%.

2. All-AlGaAs Visible (~700 nm) VCSELs

Red VCSELs have attracted much attention for their potential applications in plastic optical fiber communications, bar-code readers, chemical sensing, laser printing and displays. To date, room-temperature continuous-wave (CW) laser operation in the 650-700 nm wavelength regime has only been reported for AlGaInP materials.(see Chapter 5 of ref. [1] and references therein). An alternative to this demanding material system is to use AlGaAs alloys for both the barriers and quantum wells. Work to date for AlGaAs-based red VCSELs has been either under pulsed operation with a low duty cycle

(<2.5%)[10] or CW at low-temperature (<-25°C).[11] We demonstrated room temperature CW operation of all-AlGaAs 700 nm VCSELs for the first time.

The VCSEL samples were grown on both (100) with 2° off to (110) and (311)A GaAs substrates. Room temperature photoluminescence (PL) spectra from two calibration samples of the quantum well active layer suggests a 2.5-fold improvement of PL efficiency for the (311)A sample compared to (100) sample. This can be attributed to the quantum efficiency enhancement of interband transitions due to a large heavy-hole effective mass along the growth direction in (311)A.[12] The VCSEL structure consists of 55-periods of Si-doped $Al_{0.96}Ga_{0.04}As/Al_{0.4}Ga_{0.6}As$ *n*-type bottom DBRs, five $Al_{0.24}Ga_{0.76}As$ (80 Å)/ $Al_{0.4}Ga_{0.6}As$ quantum wells placed at the center of a one-wave thick cavity, and 30 periods of C-doped $Al_{0.96}Ga_{0.04}As/Al_{0.4}Ga_{0.6}As$ *p*-type DBRs.[13] The $Al_{0.4}Ga_{0.6}As$ barrier layer is chosen to provide enough confinement, but to avoid photo-generated carriers being trapped to the X-valley through a non-radiative relaxation. The low index layers of the DBR pairs adjacent to the cavity were $Al_{0.98}Ga_{0.02}As$, which was selectively oxidized to form a current aperture in the devices. Device characterization was performed from 5 to 50 °C.

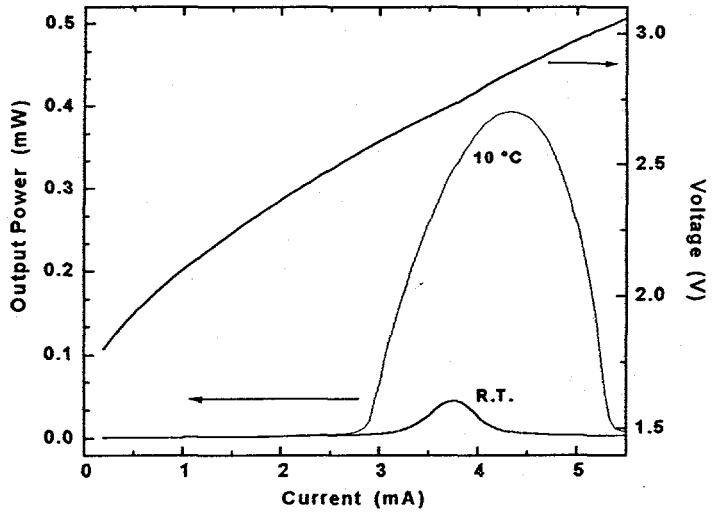

Fig. 8. L-I characteristics of a 3.8×3.8 μm^2 VCSEL at room temperature and 10 °C. The I-V data at room temperature is also shown.

Shown in Fig. 8 is the CW output power detected by a calibrated Si photodiode and the voltage across the device as a function of operating current. The data were taken at 10 °C and room temperature (21 °C) for a 3.8 μm × 3.8 μm device. Threshold current at room temperature was observed to be 3.2 mA, and the L-I curve rolls over due to thermal effects soon after reaching the peak power of 44 μW. The threshold voltage was 2.63 V. When the device is cooled to 10 °C, the threshold current dropped to 2.8 mA due to an increased PL efficiency at lower temperature and a possibly better match of the gain spectrum with the optical cavity mode. The peak power increased to 394 μW. The lasing was characterized by a clear speckle pattern from the laser and a sharp spectral feature at

705.5 nm. The full width at the half maximum is as narrow as 1.4 Å, which is limited by the resolution of the monochromator.

SUMMARY

In summary, we have demonstrated an optimized MOVPE technique for VCSEL growth. Through an *in situ* growth-rate and composition calibration, extensive doping study, and proper mirror and active layer design of the devices, highly-uniform (±0.3% wavelength variation in nearly all of the 3" wafer area) , reproducible (±0.3% over the course of 100 runs) , high efficiency (wallplug of 26%) and low threshold voltage (1.58 V) near-infrared 850-nm VCSELs were achieved. In addition, we demonstrated the first room-temperature continuous-wave operation of 700-nm red VCSELs based on AlGaAs quantum wells. Our results show the potential of MOVPE as a very stable, reproducible, and uniform growth platform for VCSEL manufacturing.

ACKNOWLEDGMENT

The authors acknowledge technical contributions from W. G. Breiland, K. M. Geib, R. J. Hickman, and J. J. Banas. This work is supported by the DOE under contract No. DE-AC04-94AL85000.

REFERENCES

[1]. See for example, *Current Trends in Vertical Cavity Surface Emitting Lasers*, Edited by T.P. Lee, World Scientific, Singapore, 1995.
[2]. W.G. Breiland and K.P. Killeen, *J. Appl. Phys.* **78**, 6726 (1995).
[3]. H. Q. Hou, W. G. Breiland, B. E. Hammons, and H. C. Chui, *Electrochemical Soc. Proc.* **96-2**, 27 (1996).
[4]. See a review, T. F. Kuech and J. M. Redwing, *J. of Cryst. Growth*, **145**, 382 (1994).
[5]. H. Q. Hou, B. E. Hammons, and H. C. Chui, *Appl. Phys. Lett.* (submitted).
[6]. N. Chand, T. Henderson, J. Klem, W. T. Masselink, R. Fisher, Y. -C. Chang, and H. Morkoc, *Phys. Rev.* **B30**, 4481 (1994).
[7]. K. L. Lear and R. P. Schneider, Jr., *Appl. Phys. Lett.* **68**, 605 (1996).
[8]. K. D. Choquette, K. L. Lear, R. P. Schneider, Jr., K. M. Geib, J. J. Figiel, and R. Hull, *IEEE Photon. Technol. Lett.* 7, 1237 (1995).
[9]. H.Q. Hou, H.C. Chui, K.D. Choquette, B.E. Hammons, W.G. Breiland, and K.M. Geib, *IEEE Photon. Technol. Lett.* **8** (1996), to be published.
[10]. B. Tell, K. F. Brown-Goebeler, and R. E. Leibenguth, *IEEE Photon. Technol. Lett.* **5**, 637 (1993).
[11]. T. E. Sale, J. S. Roberts, J. Woodhead, J. P. R. David, and P. N. Robson, *IEEE Photon. Technol. Lett.* **8**, 473 (1996).
[12]. M. Takahashi, P. Vaccaro, K. Fujita, and T. Watanabe, *Appl. Phys. Lett.* **66**, 93 (1995).
[13]. H. Q. Hou, M. Hagerott Crawford, R. J. Hickman, and B. E. Hammons, *Electron. Lett.* (submitted).